Site Selective Doping of Ultrathin Metal Dichalcogenides by Laser-Assisted Reaction

Eunpa Kim, Changhyun Ko, Kyunghoon Kim, Yabin Chen, Joonki Suh, Sang-Gil Ryu, Kedi Wu, Xiuqing Meng, Aslihan Suslu, Sefaattin Tongay, Junqiao Wu, and Costas P. Grigoropoulos**

2D transition metal dichalcogenide (TMDC) devices exhibit exceptional characteristics that are particularly suitable for next generation optoelectronic and electronic device applications.[1–3] They are excellent candidate materials for transistors,[4–6] photodectors,[7,8] electroluminescent devices,[9] and sensors.[10–14] For most of these applications, doping is needed to tune the free carrier type and density. However, previous efforts have mostly focused on doping TMDCs by means of charge transfer from adsorbed molecules,[15–19] electrostatic,[20,21] or physisorption gating,[22] defect engineering,[23,24] and substitutional doping during growth.[25] Here we report a versatile method for widely tunable, site-specific doping of ultrathin TMDCs (MoS_2 and WSe_2) through focused laser irradiation in a phosphine environment. The p-type doping with phosphorus is localized and selective, and the doping level is widely tunable by varying the duration and intensity of laser irradiation. We show the doping tendency in both n-type and p-type TMDCs by photoluminescence mapping and device characterization. This study therefore establishes a new paradigm for digitally controlled and air-stable doping of TMDCs for high-quality, and high-fidelity nanodevices.

Dr. E. Kim, Dr. S.-G. Ryu, Prof. C. P. Grigoropoulos
Laser Thermal Lab
Department of Mechanical Engineering
University of California
Berkeley, CA 94720, USA
E-mail: cgrigoro@berkeley.edu
Dr. C. Ko, Dr. Y. Chen, J. Suh,
Dr. X. Meng, Prof. J. Wu
Department of Materials Science and Engineering
University of California
Berkeley, CA 94720, USA
E-mail: wuj@berkeley.edu
Prof. K. Kim
School of Mechanical Engineering
Sungkyunkwan University
Suwon 440-746, South Korea
K. Wu, Dr. X. Meng, Dr. A. Suslu, Prof. S. Tongay
School for Engineering of Matter, Transport and Energy
Arizona State University
Tempe, AZ 85287, USA
Dr. X. Meng
Research Center for Light Emitting Diodes (LED)
Zhejiang Normal University
Jinhua 321004, P. R. China
Prof. J. Wu
Division of Materials Sciences and Engineering
Lawrence Berkeley National Laboratory
Berkeley, CA 94720, USA

DOI: 10.1002/adma.201503945

Recently, TMDCs with the general chemical formula of MX_2 (M = Mo and W; X = S, Se, and Te) have attracted much interest owing to their finite direct band gaps, rich excitonic dynamics, and valley polarization (valleytronics) associated with the broken inversion symmetry. These layered semiconductors, composed of vertically stacked layers held together by van der Waals interactions, are emerging alternatives to silicon-based electronics.[26] Despite the potential in electronics and optoelectronics, reliable and stable processing methods are needed for transition to practical applications.[27] More specifically, controlled doping of semiconductors is vital for integration into devices. Especially, for nanoscale devices using ultrathin TMDCs as an ultrathin body in devices, in order to minimize random dopant fluctuation and ensure device performance reproducibility, site-specific doping with precise doping level control becomes essential. Our method provides a systematic approach to this problem, demonstrating superior, in situ control of the spatial distribution and doping level of TMDCs.

The laser doping method has been demonstrated to produce superior device characteristics compared with other conventional methods such as implantation or diffusion.[28,29] A schematic diagram of the laser-assisted doping process is shown in **Figure 1**a. The laser serves two major functions: (i) creation of sulfur vacancies in the TMDC materials and (ii) simultaneous dissociation of the dopant molecules. The released dopant molecules are then incorporated into the vacancy sites. Phosphine (PH_3) was introduced as a p-type dopant precursor for ultrathin TMDCs where phosphorus occupies sulfur sites, in contrast to its use for n-type doping of silicon. The PH_3 doping of Si has been extensively studied both experimentally and through theoretical modeling.[30–32] Despite differences between silicon and TMDCs, it is reasonable to adopt the vacancy mechanism in the present study. Considering that the dissociation temperature of the TMDCs is in the range of 1200–1400 K, a laser power slightly below this range is enough for breaking the PH_3 molecules whose dissociation temperature is 685 K.

Figure 1b shows the optical image of mechanically exfoliated monolayer and five-layer MoS_2 flakes. The monolayer MoS_2 flake in Figure 1c is identified with a thickness of ≈0.7 nm.[4] The photoluminescence (PL) map shown in Figure 1d is taken from the laser-irradiated region indicated in Figure 1c.[33] The PL spectra of monolayer MoS_2 before and after the laser-assisted phosphorus doping are shown in **Figure 2**a. The peak PL intensity of the laser-doped area is approximately one order of magnitude greater than that of the as-exfoliated monolayer

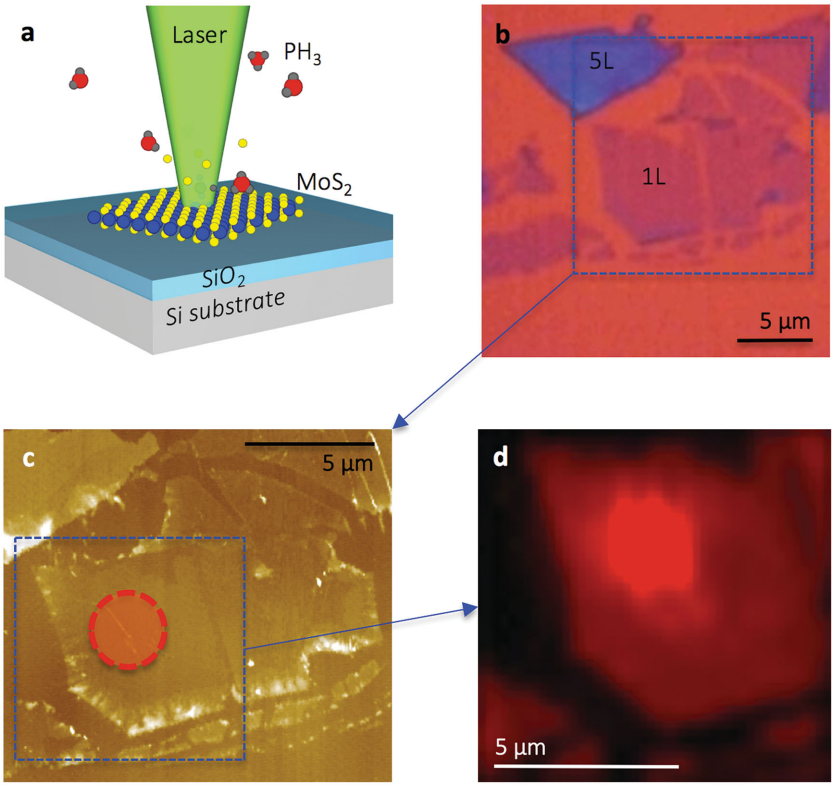

Figure 1. a) Schematic diagram of the laser-assisted doping method. b) Optical image of as-prepared monolayer MoS_2 on SiO_2/Si substrates. c) Atomic force microscopy (AFM) image of the zoomed area in (b). Its thickness is around 0.7 nm, in good agreement with the thickness of monolayer MoS_2. The circle in (c) is the laser spot area in the laser doping. d) PL mapping of the zoomed area in (c) that clearly shows the PL intensity enhancement of the laser-assisted doped area.

MoS_2. The spectral distribution of the PL also sharpens upon the laser phosphorus doping while the peak energy of the PL spectra in monolayer MoS_2 is blue-shifted by ≈32 meV. The PL peak positions are consistent with the energies of the exciton peak (X; ≈1.88 eV, e–h pair) and the negative trion peak (X^-; ≈1.84 eV, e–e–h clusters).[20] For the as-exfoliated monolayer, the PL contribution of the negative trion peak (X^-) is higher than that of the exciton peak (X), demonstrating that the material is n-type in accordance with the previous reports, presumably owing to omnipresent sulfur vacancies.[25] However, in the PL spectra of monolayer MoS_2 after phosphorus laser doping, the X peak dominates the X^- peak contribution, indicating addition of free holes to the system to improve parity between the densities of free electrons and holes. Hence, the blue shift of the PL spectrum is consistent with the hole doping effect of phosphorus that acts as an acceptor in MoS_2, resulting in a compensation of the originally n-type MoS_2.

In contrast to the intrinsically n-type MoS_2, WSe_2 is known to be intrinsically p-type.[15] Such a phosphorus doping is expected to enhance the free hole density in WSe_2. Figure 2b shows the PL spectra of monolayer WSe_2, before and after the laser-assisted phosphorus doping. The as-exfoliated monolayer WSe_2 exhibits a direct band gap at 1.67 eV. The PL intensity of doped WSe_2 is drastically reduced after the laser doping. In addition, the spectral shape of the peak broadens (by 12% in full width half maximum (FWHM)). The PL peak in monolayer WSe_2 is red-shifted by 45 meV. The PL intensity and position changes are explained by the introduction of additional free holes with the phosphorus doping. These free holes turn the original, already p-type WSe_2 flakes into more p-type, thus favoring the formation and recombination of positive trions (X^+, e–h–h clusters) over those of excitons (X, e–h pair). Similar effects were also found in another p-type TMDC, WS_2 (see the Supporting Information). We note that the laser doping process does not cause detrimental structural damage to these TMDCs under the given conditions. To identify the structural damage after laser-assisted doping of MoS_2, we conducted Raman mapping prior to single spot Raman spectrum acquisition (Figure 2a,b, inset). The Raman and PL mapping area was ≈10 × 10 μm^2, corresponding to ≈400 spots separated by 0.5 μm steps per mapping image. This procedure helps confirm that point data are indeed taken from the laser reaction spot center.

We analyze the effects of different laser processing parameters (Figure 2c,d). It is known that the laser-assisted thermochemical processing provides a convenient means for systematically and rapidly accessing a wide parameter space in a single sample configuration.[34–36] The enhancement of the PL peak intensity of monolayer MoS_2 at a fixed laser power exhibits an approximately linear dependence on the laser illumination time (Figure 2c, inset), which implies monotonically increasing hole doping over the laser illumination time. At a fixed laser power of 200 mW and exposure times of 10, 60, and 120 s with the PL intensity was enhanced by 1.6, 5, and 10 times, respectively. On the other hand, as can be seen in Figure 2d, the enhancement of PL intensity with respect to the laser power shows a threshold behavior (Figure 2d, inset). Namely, the PL intensity greatly increases from that of the as-exfoliated sample as the laser power increases from 200 to 250 mW (from 6 to 35 times, respectively), but decreases as the laser power increases to 300 mW. This implies the existence of an optimal laser power, around 250 mW, at the fixed irradiation time of 60 s. Decomposition of the monolayer MoS_2 at the laser power of 300 mW was detected by contact-mode AFM. Presumably, irradiation with the laser at the power of 300 mW raises the local temperature in excess of the decomposition temperature of monolayer MoS_2, which should be ≈900 K at the given experimental conditions considering the substrate type, the environment gas species, and the gas pressure.

The Gaussian profile of the laser beam intensity is expected to generate a spatially varying temperature distribution at the irradiation spot. Although various reports have been published on optical and thermal properties of TMDC materials,[37–40] there is still insufficient information to enable accurate prediction of the induced temperature in our laser doping process.

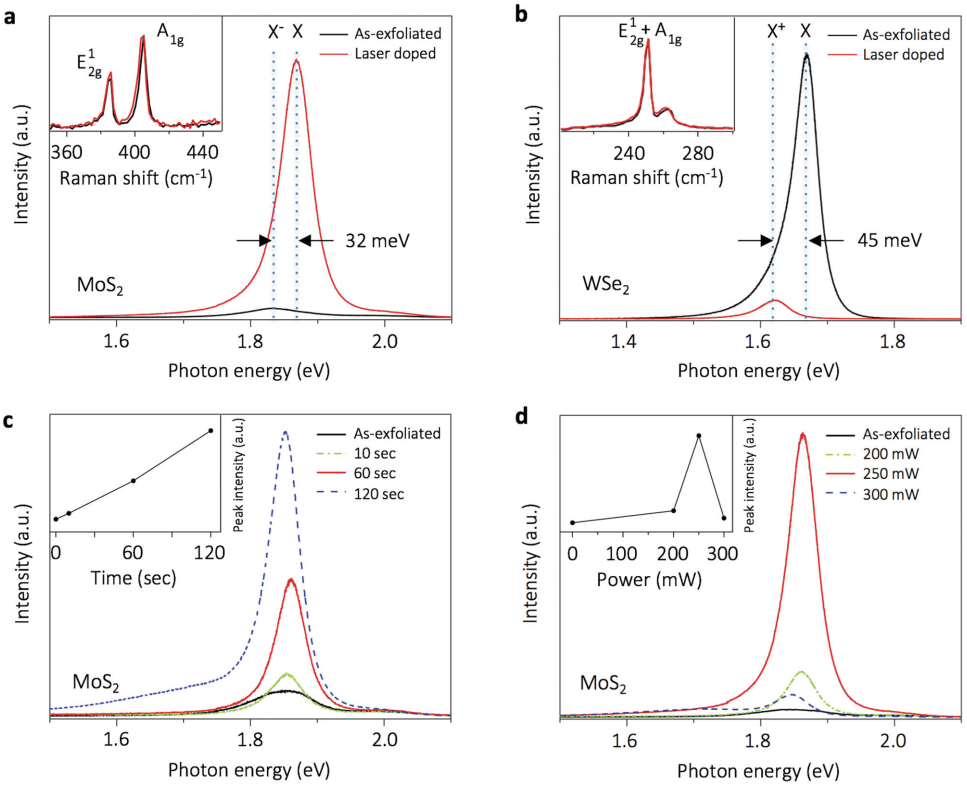

Figure 2. a) PL spectra of as-exfoliated and optimally (250 mW for 60 s, laser-doped spot center) laser-doped monolayer MoS_2. Inset: Raman spectrum of as-exfoliated and laser-doped monolayer MoS_2. b) The same spectra for monolayer WSe_2 (optimal condition is 150 mV for 60 s). c) PL change of monolayer MoS_2 with different laser doping time at a fixed laser power of 200 mW. The inset shows the peak PL intensity values as a function of the laser doping time. d) PL spectra of monolayer MoS_2 with different laser doping power at a fixed laser doping time of 60 s. The inset shows the peak PL intensity values as a function of the laser power.

The maximum PL intensities across the laser-doped regions in the monolayers MoS_2 (**Figure 3**a, inset) and WSe_2 (Figure 3b, inset) are plotted in Figure 3a,b. These distributions could be fitted to a Gaussian profile, suggesting that the hole doping concentration increases with doping temperature, which maximizes at the center of the laser reaction spot. The FWHM of the PL intensity profile was ≈2.5 µm, which is in agreement with the focal spot size of ≈2.3 µm, considering the 10× with a numerical aperture (NA) of 0.28 objective lens and the 532 nm laser light wavelength. Figure 3c, inset, shows that for MoS_2, the PL gradually shifts weight from X^- to X emission as the reaction spot is scanned from the edge to the center. In contrast, the WSe_2 shows a transition from X to X^+ (Figure 3d, inset).

Reliable performance of devices requires stable doping of the active materials. Indeed, previous studies have already achieved both n-type and p-type dopings by surface charge transfer mechanisms, mostly through chemical physisorption.[15] However, physisorption doping is unstable and decays almost completely within an hour,[17] or is retained for longer periods only if the doping environment is maintained or protected.[22] Among the various doping methods, substitutional doping of foreign elements is an effective and stable doping strategy for TMDCs.[25] In our work, the laser was used to create sulfur vacancies and locally heat up the material to crack the precursor molecules, enabling the substitution of sulfur with phosphorus. The PL data in **Figure 4**a show that the laser-assisted doping is irreversible and stable, even after exposure in air for a month. In order to test the doping stability, we also studied the effect of pure laser annealing. In this case, the monolayer MoS_2 was laser irradiated in the absence of the dopant gas at the laser power of 250 mW and an exposure time of 60 s (i.e., exactly the same conditions used for doping). As shown in Figure 4b, the PL intensity of monolayer MoS_2 increased right after the laser annealing to a level higher by an order of magnitude than the incurred by laser doping, possibly due to suppression of nonradiative recombination of excitons at defect sites created by the laser annealing.[24] However, the PL intensity drastically dropped after one week. Within two weeks, the PL intensity receded to the original level prior to laser annealing, indicating instability of the laser annealing effect. Presence of the PH_3 molecules is, therefore, needed for stable doping.

In parallel to strong modification of the luminescent properties, the laser-assisted doping also causes drastic effects on electrical properties of the ultrathin TMDCs. This was investigated using field-effect transistor (FET) devices incorporating the locally doped TMDC layers as current channels. As displayed in **Figure 5**a,d, multiple electrodes were patterned onto TMDC bilayer flakes, covering both pristine and laser-doped regions. A voltage applied through the back gate provided additional modulation of carrier density in the TMDC channel. In the undoped regions, n-type (p-type) FET behavior was observed with on–off ratio exceeding five orders of magnitude from the MoS_2 (WSe_2)

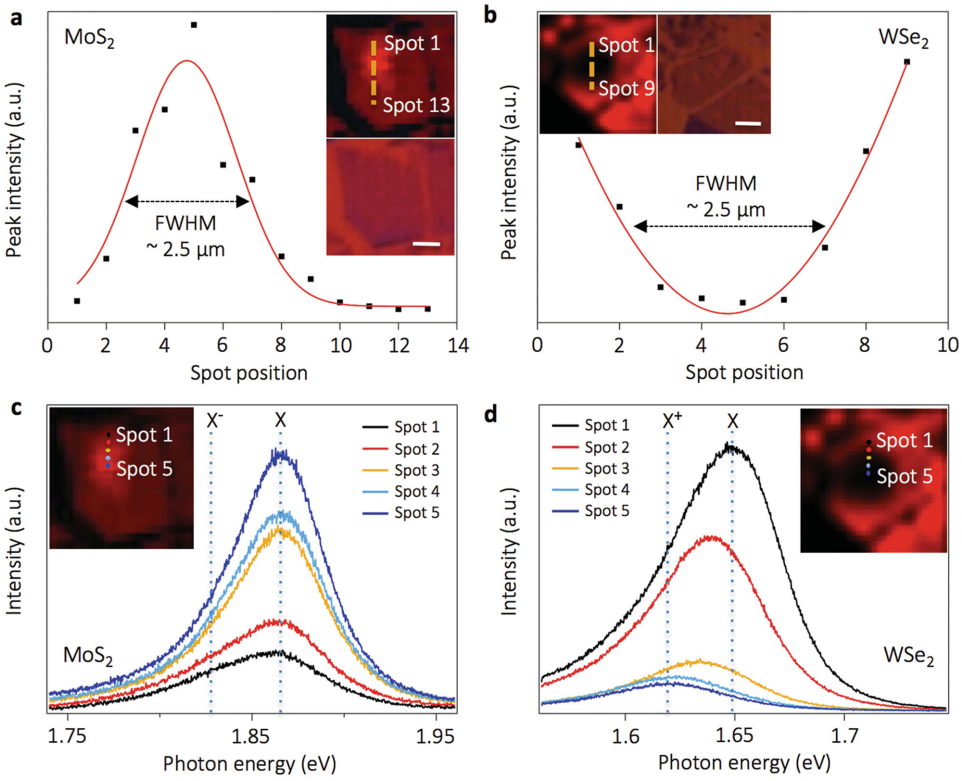

Figure 3. The PL peak intensity line profile of laser-assisted doping monolayer a) MoS_2 and b) WSe_2 at the reaction spot. Inset images show the PL peak intensity-mapping image and optical microscopy image of the laser-doped region. Scale bars are 2 and 5 μm, respectively. Variation of the PL intensity within the single spot of laser-doped monolayers c) MoS_2 and d) WSe_2. The inset shows the PL mapping image. The spacing between each spot is 500 nm.

bilayers. The FET characteristics, i.e., source–drain current (I_{SD}) versus back gate voltage (V_G) curves, of devices fabricated at different distances from the center of the laser-doped region change in a manner consistent with the spatial variation of PL across the same region, as summarized in Figure 5b,e. The phosphorus doping suppresses the n-type characteristics of the MoS_2 and enhances the p-type characteristics of the WSe_2, with increase in conductance as well as shift of threshold voltage. The hysteresis features of FET loops are likely due to water molecule absorption on the surface of the TMDCs, considering that all electrical measurements were conducted under ambient conditions.[41] In addition, the I_{SD} versus source–drain voltage (V_{SD}) curves obtained from the MoS_2 and WSe_2 channels in Figure 5c,f, respectively, further confirm introduction of acceptors by the laser treatment.

In summary, laser-assisted phosphorus doping was demonstrated on ultrathin (monolayer and bilayer) TMDCs including n-type MoS_2 and p-type WSe_2. This approach effectively introduces electronically active phosphorus atoms into the TMDCs. The precise level, temporal and spatial controls of the doping are achieved by varying the laser irradiation power and time, demonstrating wide tunability and high site selectivity. Future

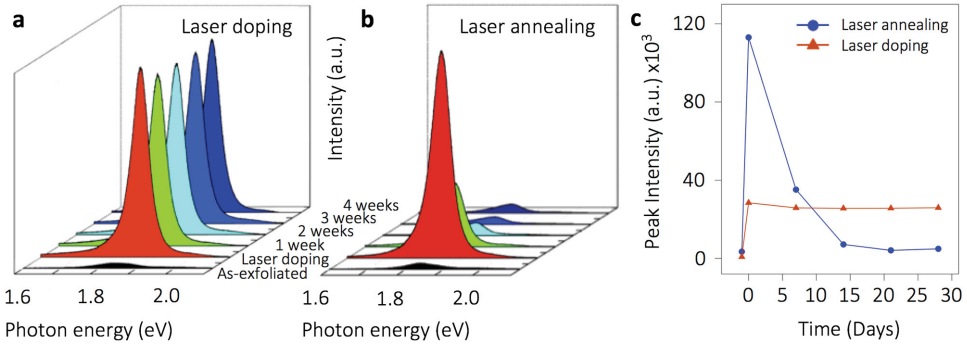

Figure 4. Long-term room-temperature stability of laser-doped monolayer MoS_2. a) PL spectra demonstrating the stability of the monolayer MoS_2 laser-assisted doped with phosphorus and b) laser annealed with the same laser power and time but under exposure to oxygen and water molecules in ambient air. c) The peak PL intensity of the laser-doped and laser-annealed monolayer MoS_2 varying over time in ambient.

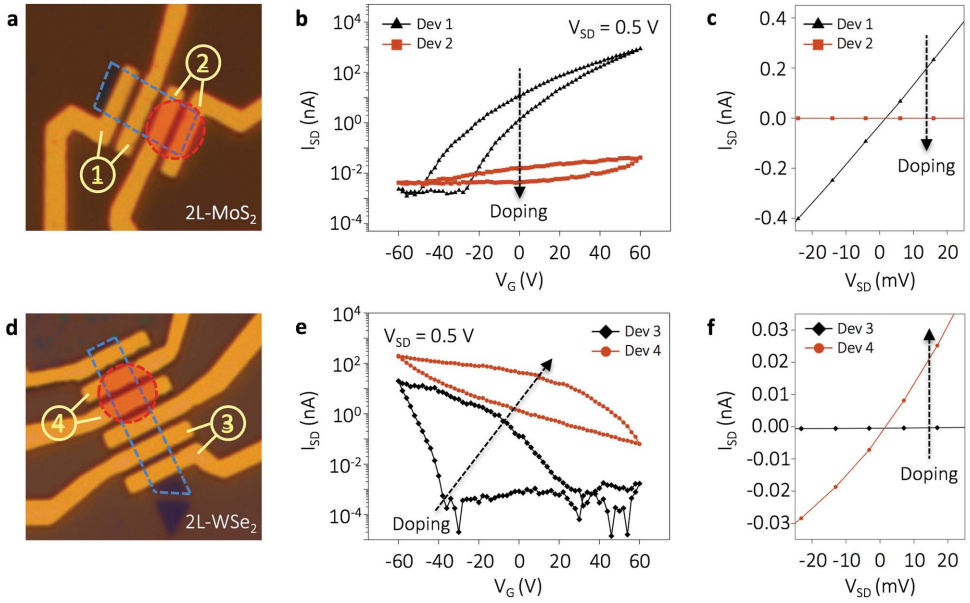

Figure 5. a,d) Bilayer MoS_2 and WSe_2 FET devices. The flakes are outlined by the blue dashed boxes and the laser-irradiated areas are denoted by the red dashed circles. b,e) Source–drain current (I_{SD}) versus back gate voltage (V_G) curves recorded from the devices in panels (a) and (d) with a bias voltage of 500 mV. c,f) Source–drain current (I_{SD}) versus source–drain voltage (V_{SD}) curves recorded from the doped (Dev 2, 4) and undoped (Dev 1, 3) devices.

investigation of the choice of dopant, the dopant concentration, and the contact engineering should be conducted. The high stability and effectiveness of the laser-assisted doping method combined with the site selectivity and tunability demonstrated here may enable a new avenue for functionalizing TMDCs for customized nanodevice applications.

Experimental Section

TMDCs Sample Preparation, MoS_2: Single and bilayer MoS_2 flakes were mechanically exfoliated from commercially available crystals of MoS_2 (SPI).

WS_2 and WSe_2: Single crystals of WX_2 were grown by vapor transport technique using iodine as the transport agent to facilitate material growth using a two-step process. In the first step, polycrystalline WSe_2 (WS_2) powders were synthesized at 1065 °C (1110 °C) for 3 d in a single-zone furnace using tungsten and selenium (sulfur) high-purity (99.995%) powders (–325 mesh) with a molar ratio of 1:2.02 ± 0.01 in evacuated quartz tubes. Samples were cooled down to room temperature at 50 °C h^{-1}. About 2.5 g of the WSe_2 (WS_2) and I_2 granule (3 mg cc^{-1}) were introduced into the quartz tubes. The quartz tube was evacuated to 2×10^{-6} Torr and sealed. Tubes were placed in a three-zone furnace and the furnace was heated to 1030 °C, 1000 °C, and 940 °C (1070 °C, 1030 °C, and 980 °C), respectively. Powders were located in the hot zone ($T_{precursor}$ = 1030 °C and 1070 °C for WS_2) and synthesized crystals were collected in the cold zone (T_{growth} = 940 °C and 980 °C for WS_2). The total duration of the growth was set to 3–4 weeks and eventually cooled down to room temperature at the rate of 50 °C h^{-1}.

Laser Doping System: The laser-assisted doping experiments were carried out in a dedicated apparatus. The system is equipped with a multichannel gas panel for doping gas supply (10 sccm of 1% PH_3) with 400 sccm Ar dilution gas and is equipped with vacuum chambers pumped to 10^{-4} Torr by a dry pump before the total pressure of 400 Torr for laser doping reaction. The laser source already in place was a highly stable continuous wave 532 nm laser (diode-pumped solid state laser, 5 W, Sprout-DTM, Lighthouse photonics) focused onto the sample in the vacuum reaction chamber, which was placed on high precision XY stage (Aerotech), by a 10× objective lens (Mitutoyo, 0.28 NA) for laser delivery.

Micro-Raman/PL Measurements: A commercially available micro-PL and Raman measurement system (Renishaw) was equipped with an Ar-ion laser (488 nm) and 1200, 2400 l mm^{-1} grating for PL and Raman, respectively. A 100× objective lens (0.95 NA) was used, and the focused laser spot size on the sample was around 0.5 μm. Typical excitation laser power was around 25 μW to avoid heating, damaging, and nonlinear optical effects. Typical measurement integration time was 10 s. All measurements were performed at room temperature.

Nano-Auger Electron Spectroscopy (Nano-AES): Nano-AES was conducted to investigated the chemical properties of locally laser-assisted doped regions using an Oxford/Omicron system where a field emission gun is equipped enabling a spatial resolution of ≈10 nm at an ultrahigh vacuum of pressure ≈10^{-10} mbar.

Device Fabrication and Electrical Characterization: Exfoliated 2D crystals were patterned into rectangular patches by XeF_2 etching subsequent to standard electron beam lithography (EBL). Then, after local laser doping, polymethylmethacrylate resist masks generated by EBL were used to deposit metal electrode channels of Pt/Au and Ti/Au (10 nm/70 nm) on the WSe_2 and MoS_2 layers, respectively, by e-beam evaporation followed by the lift-off process. Back-gated FET experiments were conducted on the probes station equipped with two Keithley 617 programmable electrometers, an NI BNC-2090 A/D board, and a current amplifier, under the ambient conditions.

Supporting Information

Supporting Information is available from the Wiley Online Library or from the author.

Acknowledgements

C.K. and K.K. contributed equally to this work. The authors thank Taegyun Park for his assistance in sample preparation. Support from the US Air Force Office of Scientific Research AFOSR/AOARD under

grant FA2386-13-4123 is gratefully acknowledged. This work was also partially supported by the National Science Foundation under Grant No. DMR-1306601. Nano-Auger experiment at the Molecular Foundry was supported by the Office of Science, Office of Basic Energy Sciences, of the U.S. Department of Energy under Contract No. DE-AC02-05CH11231. The laser-induced doping was conducted on the LACVD apparatus in the UC Berkeley Marvell Nanofabrication Laboratory.

Received: August 13, 2015
Revised: September 21, 2015
Published online: November 16, 2015

[1] Q. H. Wang, K. Kalantar-Zadeh, A. Kis, J. N. Coleman, M. S. Strano, *Nat. Nanotechnol.* **2012**, *7*, 699.
[2] D. Jariwala, V. K. Sangwan, L. J. Lauhon, T. J. Marks, M. C. Hersam, *ACS Nano* **2014**, *8*, 1102.
[3] R. Ganatra, Q. Zhang, *ACS Nano* **2014**, *8*, 4074.
[4] B. Radisavljevic, A. Radenovic, J. Brivio, V. Giacometti, A. Kis, *Nat. Nanotechnol.* **2011**, *6*, 147.
[5] H. Wang, L. L. Yu, Y. H. Lee, Y. M. Shi, A. Hsu, M. L. Chin, L. J. Li, M. Dubey, J. Kong, T. Palacios, *Nano Lett.* **2012**, *12*, 4674.
[6] S. Kim, A. Konar, W. S. Hwang, J. H. Lee, J. Lee, J. Yang, C. Jung, H. Kim, J. B. Yoo, J. Y. Choi, Y. W. Jin, S. Y. Lee, D. Jena, W. Choi, K. Kim, *Nat. Commun.* **2012**, *3*, 1011.
[7] O. Lopez-Sanchez, D. Lembke, M. Kayci, A. Radenovic, A. Kis, *Nat. Nanotechnol.* **2013**, *8*, 497.
[8] Z. Yin, H. Li, H. Li, L. Jiang, Y. Shi, Y. Sun, G. Lu, Q. Zhang, X. Chen, H. Zhang, *ACS Nano* **2012**, *6*, 74.
[9] J. S. Ross, P. Klement, A. M. Jones, N. J. Ghimire, J. Yan, D. G. Mandrus, T. Taniguchi, K. Watanabe, K. Kitamura, W. Yao, D. H. Cobden, X. Xu, *Nat. Nanotechnol.* **2014**, *9*, 268.
[10] Q. Y. He, Z. Y. Zeng, Z. Y. Yin, H. Li, S. X. Wu, X. Huang, H. Zhang, *Small* **2012**, *8*, 2994.
[11] H. Li, Z. Y. Yin, Q. Y. He, H. Li, X. Huang, G. Lu, D. W. H. Fam, A. I. Y. Tok, Q. Zhang, H. Zhang, *Small* **2012**, *8*, 63.
[12] B. Cho, M. G. Hahm, M. Choi, J. Yoon, A. R. Kim, Y. J. Lee, S. G. Park, J. D. Kwon, C. S. Kim, M. Song, Y. Jeong, K. S. Nam, S. Lee, T. J. Yoo, C. G. Kang, B. H. Lee, H. C. Ko, P. M. Ajayan, D. H. Kim, *Sci. Rep.* **2015**, *5*, 8052.
[13] B. Cho, A. R. Kim, Y. Park, J. Yoon, Y. J. Lee, S. Lee, T. J. Yoo, C. G. Kang, B. H. Lee, H. C. Ko, D. H. Kim, M. G. Hahm, *ACS Appl. Mater. Interfaces* **2015**, *7*, 2952.
[14] B. Cho, J. Yoon, S. K. Lim, A. R. Kim, D. H. Kim, S. G. Park, J. D. Kwon, Y. J. Lee, K. H. Lee, B. H. Lee, H. C. Ko, M. G. Hahm, *ACS Appl. Mater. Interfaces* **2015**, *7*, 16775.
[15] S. Mouri, Y. Miyauchi, K. Matsuda, *Nano Lett.* **2013**, *13*, 5944.
[16] H. Fang, S. Chuang, T. C. Chang, K. Takei, T. Takahashi, A. Javey, *Nano Lett.* **2012**, *12*, 3788.
[17] H. Fang, M. Tosun, G. Seol, T. C. Chang, K. Takei, J. Guo, A. Javey, *Nano Lett.* **2013**, *13*, 1991.
[18] P. D. Zhao, D. Kiriya, A. Azcatl, C. X. Zhang, M. Tosun, Y. S. Liu, M. Hettick, J. S. Kang, S. McDonnell, K. C. Santosh, J. H. Guo, K. Cho, R. M. Wallace, A. Javey, *ACS Nano* **2014**, *8*, 10808.
[19] A. Tarasov, S. Y. Zhang, M. Y. Tsai, P. M. Campbell, S. Graham, S. Barlow, S. R. Marder, E. M. Vogel, *Adv. Mater.* **2015**, *27*, 1175.
[20] K. F. Mak, K. L. He, C. Lee, G. H. Lee, J. Hone, T. F. Heinz, J. Shan, *Nat. Mater.* **2013**, *12*, 207.
[21] B. Radisavljevic, A. Kis, *Nat. Mater.* **2013**, *12*, 815.
[22] S. Tongay, J. Zhou, C. Ataca, J. Liu, J. S. Kang, T. S. Matthews, L. You, J. B. Li, J. C. Grossman, J. Q. Wu, *Nano Lett.* **2013**, *13*, 2831.
[23] S. Tongay, J. Suh, C. Ataca, W. Fan, A. Luce, J. S. Kang, J. Liu, C. Ko, R. Raghunathanan, J. Zhou, F. Ogletree, J. B. Li, J. C. Grossman, J. Q. Wu, *Sci. Rep.* **2013**, *3*, 2657.
[24] H. Y. Nan, Z. L. Wang, W. H. Wang, Z. Liang, Y. Lu, Q. Chen, D. W. He, P. H. Tan, F. Miao, X. R. Wang, J. L. Wang, Z. H. Ni, *ACS Nano* **2014**, *8*, 5738.
[25] J. Suh, T. E. Park, D. Y. Lin, D. Fu, J. Park, H. J. Jung, Y. Chen, C. Ko, C. Jang, Y. Sun, R. Sinclair, J. Chang, S. Tongay, J. Wu, *Nano Lett.* **2014**, *14*, 6976.
[26] A. K. Geim, I. V. Grigorieva, *Nature* **2013**, *499*, 419.
[27] S. Z. Butler, S. M. Hollen, L. Y. Cao, Y. Cui, J. A. Gupta, H. R. Gutierrez, T. F. Heinz, S. S. Hong, J. X. Huang, A. F. Ismach, E. Johnston-Halperin, M. Kuno, V. V. Plashnitsa, R. D. Robinson, R. S. Ruoff, S. Salahuddin, J. Shan, L. Shi, M. G. Spencer, M. Terrones, W. Windl, J. E. Goldberger, *ACS Nano* **2013**, *7*, 2898.
[28] T. Sameshima, S. Usui, H. Tomita, *Jpn. J. Appl. Phys.* **1987**, *26*, L1678.
[29] D. J. Ehrlich, R. M. Osgood, T. F. Deutsch, *Appl. Phys. Lett.* **1980**, *36*, 916.
[30] P. A. Taylor, R. M. Wallace, W. J. Choyke, J. T. Yates, *Surf. Sci.* **1990**, *238*, 1.
[31] P. J. Chen, M. L. Colaianni, R. M. Wallace, J. T. Yates, *Surf. Sci.* **1991**, *244*, 177.
[32] H. F. Wilson, O. Warschkow, N. A. Marks, N. J. Curson, S. R. Schofield, T. C. G. Reusch, M. W. Radny, P. V. Smith, D. R. McKenzie, M. Y. Simmons, *Phys. Rev. B: Condens. Matter* **2006**, *74*, 195310.
[33] A. Splendiani, L. Sun, Y. B. Zhang, T. S. Li, J. Kim, C. Y. Chim, G. Galli, F. Wang, *Nano Lett.* **2010**, *10*, 1271.
[34] D. J. Hwang, S. G. Ryu, C. P. Grigoropoulos, *Nanotechnology* **2011**, *22*, 385303.
[35] D. J. Hwang, S. G. Ryu, E. Kim, C. P. Grigoropoulos, C. Carraro, *Appl. Phys. Lett.* **2011**, *99*, 123109.
[36] S. G. Ryu, E. Kim, J. H. Yoo, D. J. Hwang, B. Xiang, O. D. Dubon, A. M. Minor, C. P. Grigoropoulos, *ACS Nano* **2013**, *7*, 2090.
[37] C. Y. Yim, M. O'Brien, N. McEvoy, S. Winters, I. Mirza, J. G. Lunney, G. S. Duesberg, *Appl. Phys. Lett.* **2014**, *104*, 103114.
[38] X. J. Liu, G. Zhang, Q. X. Pei, Y. W. Zhang, *Appl. Phys. Lett.* **2013**, *103*, 133113.
[39] C. Muratore, V. Varshney, J. J. Gengler, J. J. Hu, J. E. Bultman, A. K. Roy, B. L. Farmer, A. A. Voevodin, *Phys. Chem. Chem. Phys.* **2014**, *16*, 1008.
[40] R. S. Yan, J. R. Simpson, S. Bertolazzi, J. Brivio, M. Watson, X. F. Wu, A. Kis, T. F. Luo, A. R. H. Walker, H. G. Xing, *ACS Nano* **2014**, *8*, 986.
[41] D. J. Late, B. Liu, H. S. S. R. Matte, V. P. Dravid, C. N. R. Rao, *ACS Nano* **2012**, *6*, 5635.